Proceedings of the 25th International Conference on
Port and Ocean Engineering under Arctic Conditions
June 9-13, 2019, Delft, The Netherlands

Mechanism of shear collapse in sea ice

A. Sakharov[1], E. Karulin[2], A. Marchenko[3,4], M. Karulina[2] , P. Chistyakov[1]

[1] Moscow State University, Moscow, RUSSIA

[2]Krylov State Research Centre, St.-Petersburg, RUSSIA

[3]The University Centre in Svalbard, Longyearbyen, Norway

[4] Norwegian University of Science and Technology, Trondheim, Norway

ABSTRACT

The results of full-scale shear tests of the sea ice *in-situ* in Van-Mijen fiord of Spitsbergen are presented in the paper. The shear strength of the sea ice has been investigated in details by various groups of researchers (Frederking and Timco, 1984, 1986; Saeki, et al., 1985). Focus of our study is the shear collapse or *self-confinement effect* resulting in the appearance of a compression in transversal direction to the shear surface. It is found that the plastic shear mechanism can be locked by compression due to dilatancy in constraint stress states.

We propose the model of the sea ice dilatancy on the frame of two concepts. Firstly we use the macroscopic incremental theory of dilatant hardening material (Rudnicki and Rice, 1975; Rice, 1975). It allows to describe the self-confinement effect and underline the differences between shear fault and punching. The second concept is microscopic theory based on the "wing cracks" mechanism in ice (Schulson, 2002), where the irreversible volume strain and shear deformation occur during the nucleation and development of microcracks. This "wing crack" mechanism is used for estimation of the dilation coefficient value in ice.

The ice behavior under shear is investigated in keeping of this approach. The results of our shear tests are compared with the tests results of other research groups.

KEY WORDS: Dilation: Wing-crack mechanism: Incremental theory: Shear strength of the sea ice.

INTRODUCTION

Shear strength is used in the horizontal pressure calculation on coastal structures as well as for estimation of the sea ice sheet bearing capacity. There are few testing methods to measure the shear strength – four-point asymmetric loading test (fig 1a) and direct shearing test (fig.1b). The first schema is convenient for field measurement of the shear strength and the second – for lab tests. In both tests the shear strength is calculated as $\tau_s = P_s / A$, where P_s is ultimate shear load, A is total area of the sample in shear plane. Also the direct shear test was applied to estimate the influence of compression stress $\sigma_v = P_c / A$ on the shear strength. According to the *principal of effective stress* in soil mechanics (Wisley, 2009) the relation between shear strength τ and compression σ_v on shear plane was proposed as Coulomb's equation $\tau = \tau_s + \mu \sigma_v$

where τ_s - cohesive strength (pure shear strength), $\mu = tg\,\psi$, ψ is the angle of internal friction and μ is the coefficient of static friction.

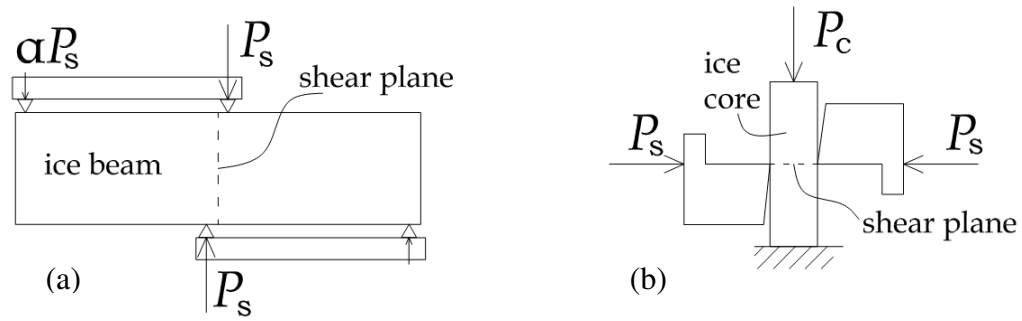

Fig.1 (a) four-point asymmetric shear test (Frederking et al, 1984), (b) direct shear strength test (Saeki, et al., 1985).

The results of five years sea ice experiments (Saeki, et al., 1985) allow to conclude that cohesive strength of the sea ice in the range of temperature *T= -2…-9 C⁰* and in the range of salinity *2,5-6,0 ppt* follow the linear relation $\tau_s = 150 - 93 * T\left(C^0\right)$, *kPa* with high accuracy (table 1).

Table 1 (data from Saeki H. et al, 1985)

T, C^0	-2	-3	-4	-5	-6	-7	-8	-9
τ_s, kPa	340	430	530	620	710	800	900	990

These data are in a good agreement with the average value of shear strength 1100 kPa at T=-10⁰C (Frederking et al, 1988) at four-point asymmetric loading tests (fig.1a). Special stress relief material at the load application points was used for reducing stress concentrations. Earlier in double shear tests the similar results were obtained by Butkovich (1956).

Tests with the independent biaxial loading also allow to estimate the coefficient of internal friction. In direct shear strength tests (Saeki et al, 1985) in the temperature range of *T= -2…-20 C⁰* and the salinity range of *2,5-6,0 ppt* the coefficient of friction μ was in range 0.1 to 1.3 (for low temperature -20⁰C) and follow the relation $\mu = 0{,}06 - 0{,}06 * T\left(C^0\right)$.

The proportional biaxial compression stress with different ratio *R* of principal stresses $R = \sigma_3 / \sigma_1$ allowed completing brittle failure envelope for first-year sea ice in the compressive quadrant (Schulson et al, 2006). It was obtained that under lower confinement R<0.2 the ice failed by Coulumbic shear faulting (fig.2). The same failure type was observed in our shear test, where $\sigma_3 \cdot \sigma_1 < 0$ *and* $|\sigma_3| < \sigma_1$. Another failure type – punching (Photo 1) was observed in the fixed-ends bending beam test with relatively short beam (Marchenko, 2014). The difference between the two modes is discussed below.

If the confinement R reaches the critical value (Schulson, 2001; Wilchinsky et al, 2011),

$$R_c^* = \frac{\left(1+\mu^2\right)^{1/2} - \mu}{\left(1+\mu^2\right)^{1/2} + \mu} \quad (1)$$

the shear faulting couldn't occur, ice would be failed by splitting or spalling.

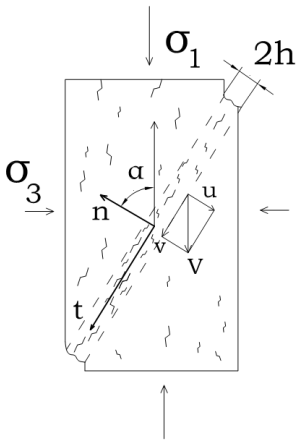

Fig.2 Shear faulting in biaxial compression test

Photo 1. Punching in the fixed-ends beam test (short beam)

The confinement (or lateral compression) *R* plays the significant role in the shear test. But the confinement could be changed during the loading due to ice dilatancy effect (*self-confinement effect).* Below we discuss this dilatancy process in the ice in the frame of macrostructure and microstructure theories.

ESTIMATION OF THE DILATANCY COEFFICIENT

The dilatancy as a physical effect plays the significant role in the class of brittle and quasi-brittle materials such as rocks (granite, limestone, etc.) and ice. The dilatancy coefficient is defined as $\beta = d\theta^p / d\gamma^p$, where $d\gamma^p = \sqrt{\frac{2}{3}}\sqrt{\left(d\varepsilon_1^p - d\varepsilon_2^p\right)^2 + \left(d\varepsilon_1^p - d\varepsilon_3^p\right)^2 + \left(d\varepsilon_3^p - d\varepsilon_2^p\right)^2}$ is the shear strain intensity, $d\theta^p = dV^p / V = -\left(d\varepsilon_1^p + d\varepsilon_2^p + d\varepsilon_3^p\right)$ is the relative inelastic volume change .

There are only few tests from which the dilatancy coefficient of ice could be estimated. In triaxial tests $\left(\sigma_1 > \sigma_2 = \sigma_3\right)$ with rectangular shaped fresh water ice specimens (Rist et al, 1997), it was found that dilatancy effect is sensitive to the strain rate. If loading is performed with high strain rate $10^{-2}s^{-1}$ the ice sample failed in shear with very small dilatancy (plots on fig.3a). It happens abruptly, failure was reached in less than 0,5ms, coinciding with fault propagation (P-fault according Golding et al, 2014).

In tests with low strain rate $10^{-4}s^{-1}$ the volumetric changes due to microcracking mechanism are observed and are associated with ductile type failure. The triaxial tests conducted by Golding (Golding et al, 2014) showed that behavior of freshwater ice and salt water ice at strain rate 10^{-2} s^{-1} and over was undistinguishable. When ice was failed in P-fault the dilatancy is quite small $\beta \cong 0{,}15...0{,}3$ (fig 3b). The average value of dilatancy coefficient is estimated as $\beta = -d\theta^p / d\gamma^p \cong 1{,}4$ from this ductile type flow test. It means that ductile and brittle type of ice fracture are based on different microstructure mechanisms.

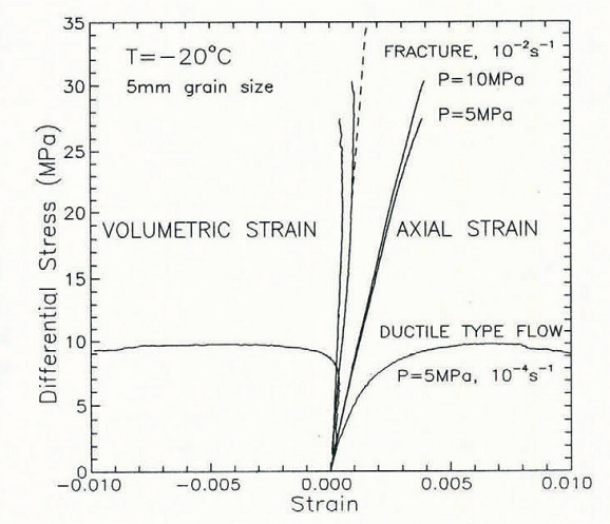

Fig. 3a. Typical plots: stress vs t (s) and strain vs t freshwater columnar ice at T=-20^{0}C at strain rate 10^{-2} and 10^{-4} s^{-1}. Rectangular shaped specimens 60*60*120 mm on edge (Rist et al, 1997). The volumetric strain curve has a plateau associated with ductile type failure; differential stress $\sigma_1 - \sigma_3$ in this test is in range 10 MPa.

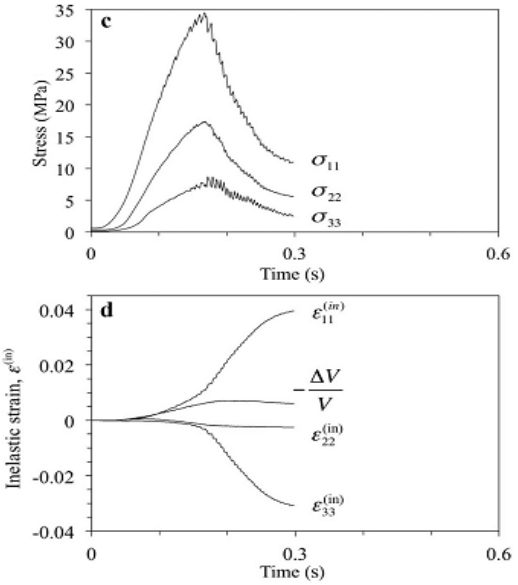

Fig. 3b. Typical plots: stress vs t (s) and inelastic strain vs t. Cube shaped specimens 100 mm on edge (Golding et al, 2014) salt water columnar ice at T=-20^{0}C at strain rate 0.05 to 0.1s^{-1}

MACROSCOPIC THEORY OF SELF-CONFINEMENT EFFECT

The macroscopic theory for dilatant hardening material is appropriate for this purpose. The constitutive equation for shear in a layer could be written (Rice, 1975)

$$d\gamma = d\gamma^e + d\gamma^p = \frac{d\tau}{G} + \frac{1}{H}\left(d\tau - \mu\, d\sigma\right) \qquad (2)$$

$$d\varepsilon = d\varepsilon^e + d\varepsilon^p = \frac{d\sigma}{E} - \beta\, d\gamma^p \qquad (3)$$

where $d\gamma$, $d\varepsilon$ are the shear and lateral strain increment in a layer; $d\tau$,$d\sigma$ are the shear and normal stresses increment and $d\tau - \mu\, d\sigma$ is the effective stress increment; G,E – shear and Young's modulus $(G=E/2(1+\nu))$; ν-Poison ratio; β, μ – the dilatancy and friction coefficients, accordingly; modulus H is declared further. The ratio of plastic dilation increment $d\varepsilon^p$ and plastic shear increment $d\gamma^p$ depends little on ratio $d\tau / d\sigma$, so long as the continuum follows the plastic law.

On fig.4a the function $\tau = \varphi(\gamma, \sigma)$ for different levels of compression stress is plotted. For increments we have $\Delta\tau = \varphi_\gamma \Delta\gamma + \varphi_\sigma \Delta\sigma$, and in case $\Delta\sigma = 0$ the tangent shear modulus is declared as

$$\left.\frac{d\tau}{d\gamma}\right|_{\Delta\sigma=0} = \varphi_\gamma = G'\left(\gamma^p, \sigma\right) \qquad (4)$$

Let's formulate the condition of active process $\Delta\gamma^p > 0$. For different ratio $\Delta\sigma / \Delta\tau$ we have the active loading paths AD $\left(\Delta\sigma = 0;\ \Delta\tau > 0;\ \Delta\gamma^p > 0\right)$ and AC $\left(\Delta\tau - \mu\Delta\sigma > 0;\ \Delta\gamma^p > 0\right)$

(Fig. 4b) and the passive loading path AB $\left(\Delta\gamma^p = 0;\ \Delta\tau = G\Delta\gamma\right)$, for path AB we have $\Delta\tau = \mu \cdot \Delta\sigma;\ \ \Delta\tau > 0$. For path AB we can write $\Delta\tau = \varphi_\sigma\,\Delta\sigma + \dfrac{\varphi_\gamma \Delta\tau}{G}$, that's why the coefficient of friction is determined from the shear test

$$\mu = \frac{\varphi_\sigma}{1 - G'/G} \tag{5}$$

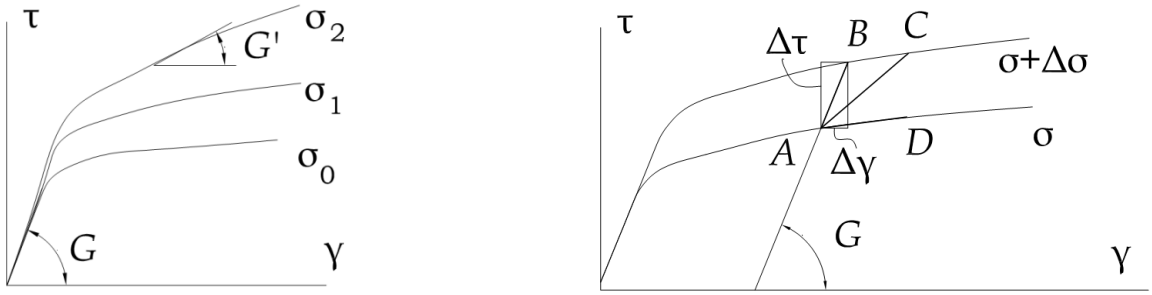

Fig.4. a – the set of shear deformation curves; b- loading pathes (AC, AD are active, AB is a passive path).

For normally hardening material $\left(G' \geq 0\right)$ from (5) follows $\mu > \varphi_\sigma$. Consider (4) and (5) we find that $\tau(\sigma,\,\gamma) = \mu\sigma - \dfrac{\mu}{G}\int G'(\sigma,\,\gamma)d\sigma + \int G'(\sigma,\gamma)\,d\gamma$. The shear increment satisfies an equation $\Delta\tau = \varphi_\sigma\,\Delta\sigma + G'\left(\Delta\gamma^p + \Delta\tau/G\right)$, and the H modulus for active process $\left(\Delta\tau/\Delta\sigma > \mu\right)$ will be equal $\dfrac{1}{H\left(\sigma,\,\gamma^p\right)} = \dfrac{1}{G'\left(\sigma,\,\gamma^p\right)} - \dfrac{1}{G}$ and

$$\Delta\gamma^p = \begin{cases} \left(\dfrac{1}{G'\left(\sigma,\ \gamma^p\right)} - \dfrac{1}{G}\right)\left(\Delta\tau - \mu\,\Delta\sigma\right), & \text{if } \Delta\tau - \mu\,\Delta\sigma > 0 \\ 0, & \text{if } \Delta\tau - \mu\,\Delta\sigma \leq 0 \end{cases} \tag{6}$$

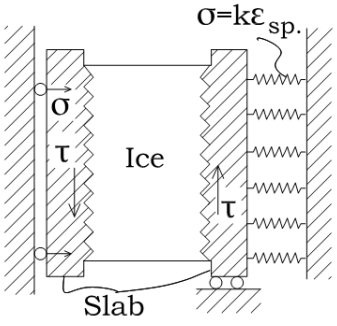

Fig.5. Shear test under confinement

Hereafter the tangent modulus G' interpolation in power order form is used

$$G'\left(\sigma,\gamma^p\right) = \frac{A}{\left(1+\gamma^p\right)^{\alpha 1}}\left(1 + \frac{\sigma}{\sigma_*}\right)^{\alpha 2} \tag{7}$$

where $0 < \alpha_1 \leq 1;\ \ \alpha_2 > 0$.

The model of the self-confinement effect in the shear test is shown on fig.5. The ice sample is loaded with displacement control under both shearing and lateral compression.

The plastic shear deformation generates the lateral strain $\Delta\varepsilon^p = -\beta\Delta\gamma^p$ and the springs develop the compression force as a reaction (active process, loading path AC fig.4b).

Using evident kinematic equation for model $\Delta\varepsilon^p + \Delta\varepsilon^e + \Delta\varepsilon_{sp.} = 0$ we receive $\Delta\varepsilon^p = -\Delta\sigma/\lambda$ where $1/\lambda = 1/E + 1/k$, λ is summed rigidity.

Taking into account $\Delta\sigma = \lambda\beta\Delta\gamma^p$ and (6) it is written $\Delta\sigma = \dfrac{\Delta\tau}{\mu + H/\beta\lambda}$ and then the equation for increments will be

$$\Delta\tau = \frac{\Delta\gamma}{(1/G + 1/(\mu\beta\lambda + H))} \qquad (8)$$

On fig.6a integral curve τ *vs* γ eq. (8) (tau_conf) and the set of curves with $\sigma = \sigma_k = const$ are plotting for compare.

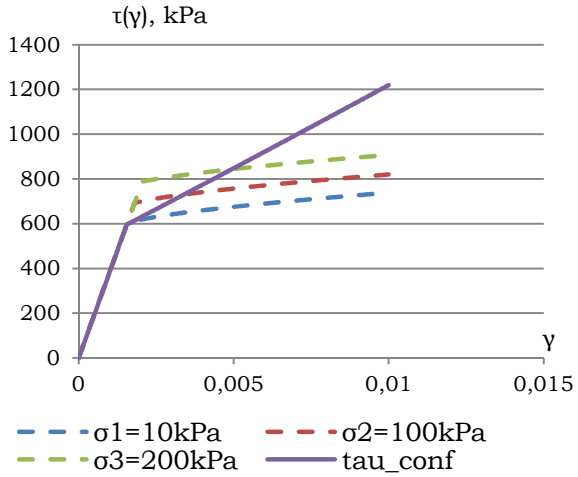

Fig.6a The plots τ *vs* γ (dot line without confinement)

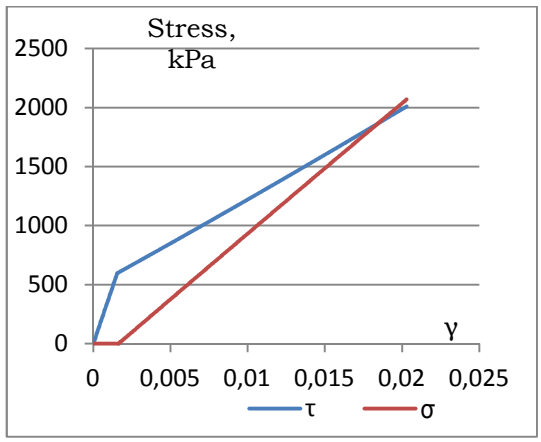

Fig.6b. The plots τ *vs* γ and σ *vs* γ underlying the self-confinement effect

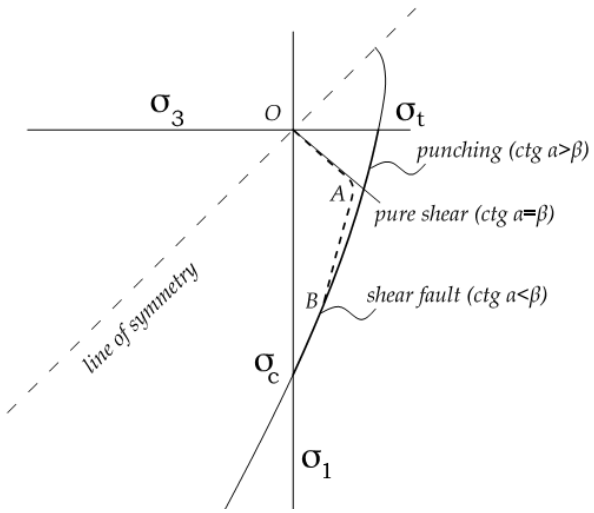

Fig.7. Failure envelope and trajectory OAB on the self-confinement test.

The lateral compression stress σ in the model is growing rapidly (fig.6b). It means that the first principal (compression) value $\sigma_1 = 1/2\left(\sigma + \sqrt{\sigma^2 + 4\tau^2}\right)$ is increasing and the third principal stress value (tension) $\sigma_3 = 1/2\left(\sigma - \sqrt{\sigma^2 + 4\tau^2}\right)$ is decreasing. The trajectory of loading OAB is shown on fig.7 in conjunction with failure envelope (Schulson et al, 2006) on the plain (σ_1, σ_2). The pure shear strength is essentially lower than the ultimate shear strength in the tests with self-confinement effect.

The macroscopic theory, based on (2)-(3), is used to determine the difference between punching and shear fault. Let's propose that shear is localizing in a narrow zone of 2h width (as it is shown on fig. 2) and the velocity components with high gradient across this zone are continuous. Also we propose that the gradient of velocity $\partial\vec{U}/\partial t << \partial\vec{U}/\partial n$, and

assume that elastic deformation is neglected. The rate of shear deformation γ^p and dilation Θ^p are expressed

$$\dot{\theta}^p = \dot{\varepsilon}_n^p = \dot{\varepsilon}_n = \partial u / \partial n, \; ; \; d\varepsilon_t^p = 0 \qquad \dot{\gamma}^p = \gamma_{nt} = \partial v / \partial n,$$

where $v = V \sin\alpha; u = V \cos\alpha$, that's why $\dot{\theta}^p = \dot{\varepsilon}_n^p = -\frac{V\cos\alpha}{2h}$; $\dot{\gamma}^p = \gamma_{nt} = \frac{V\sin\alpha}{2h}$.

According (2) it is found

$$\frac{\dot{\theta}^p}{\dot{\gamma}^p} = -\beta = -ctg\,\alpha \qquad (9)$$

It means, that compatibility of strains takes place if $\beta = ctg\,\alpha$. In another case some additional stresses will occur.

If $ctg\,\alpha < \beta$ than shear dominates and produces the volume strain more than it could be agreed with kinematic. Across the shear zone compression stress appears. This failure mode is named shear faulting (fig.8).

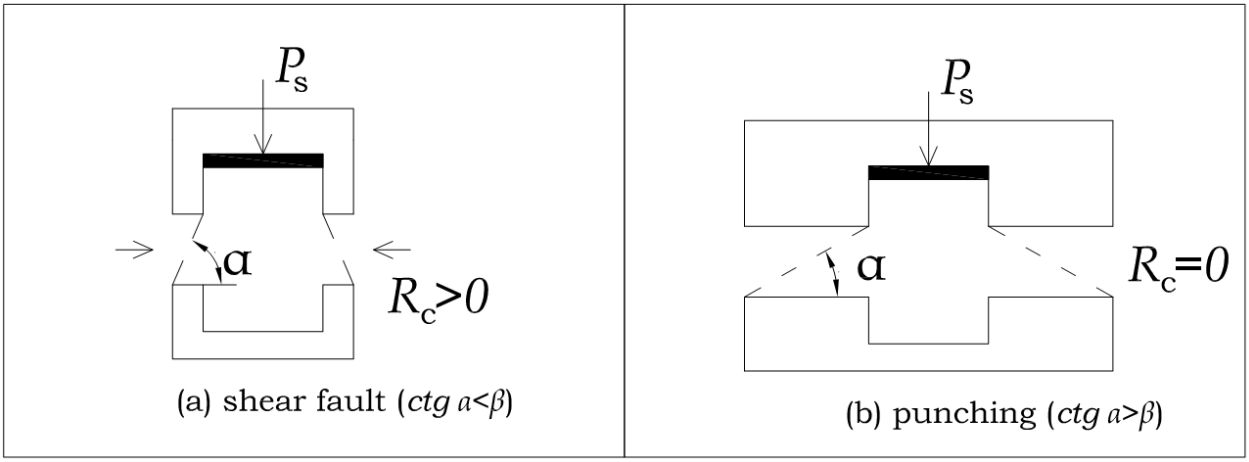

Fig.8. (a) failure mode – shear fault; (b) failure mode – punching.

If $ctg\,\alpha > \beta$ than elongation across the shear area dominates, and additional compression forces couldn't occur $(R_c = 0)$.

MICROSCOPIC THEORY BASED ON THE "WING CRACK" MECHANISM

The frictional sliding wing-crack mechanism is fruitful for understanding the ice failure phenomena under shear and compression (Schulson, 2002; Schulson et al, 2006). An initial crack in the ice under compression is subjected to stress which tries to slide in shear (Sanderson, 1988). This creates tensile areas at the two ends of the sliding spot and leads to wing cracks formation (fig.9a). Wing crack propagation conforms to the rule: tip of the crack moves along the trajectory of first principal stress (maximum compression σ_1) and crack opening follows the minimal principal stress σ_3.

Follow Lehner and Kachanov (1996) wing crack is analyzed - as "displacement-driven" and "force-driven" crack. The stress intensity factor (SIF) on crack tip for displacement-driven crack is determined ("thin rigid wedge" (3.12) Tada et al, 2000; Barenblatt and Cherepanov, 1960)

$$K_1 = \frac{E\, b \cos\alpha}{\left(1-\nu^2\right)\sqrt{2\pi l}} + \sigma_3\sqrt{\pi l/2} \qquad (10)$$

And for "force-driven" crack (Tada et al, 2000)

$$K_1 = \frac{P\cos\alpha}{\sqrt{\pi l}} + \sigma_3\sqrt{\pi l} \qquad (11)$$

where $P = 2a\tau_{eff}$ is a total force according to the principal of efficient stress $\tau_{eff} = \tau_n - \mu\sigma_n$, l is a crack length, the sign of the second term (11) is positive if σ_3 is tensile stress.

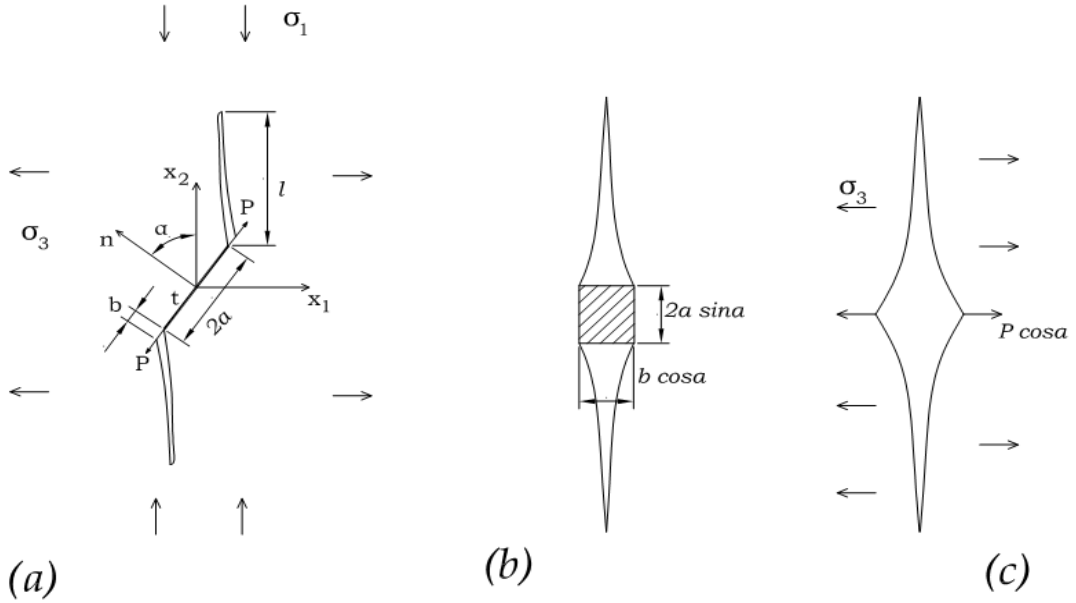

Fig.9. (a) – schema of "wing crack" mechanism; (b) "displacement-driven crack" is initiated by "thin rigid wedge"; (c) "force-driven" crack.

If the process is active, then $K_1 = K_{1C}$ and $\delta K_1 = 0$, that's why $\delta\left(\frac{b}{\sqrt{l}}\right) = 0$ or $\frac{\delta b}{b} = \frac{\delta l}{2l}$

Increment of irreversible work could be expressed

$$\delta A_p = \delta A_f + \delta A_c + \delta\Pi_d \qquad (12)$$

where $\delta A_f = 2a\mu\sigma_n\delta b$ - part of plastic work due to friction on sliding spot;

$\delta A_c = 2G_{1C}\delta l$ - part due to crack propagation, $G_{1C} = \frac{\left(1-\nu^2\right)K_{1C}^2}{E}$

$\delta\Pi_d = 2a\tau_{eff}\delta b$ - part of elastic energy due to Burger's vector along the sliding surface (fig.9), where $\delta\bar{b}; -\delta\bar{b}$ are the edge dislocations increments $\left(\bar{b}, \left(z = re^{i\alpha} - z_0\right); -\bar{b}, \left(z = re^{i\alpha} + z_0\right)\right)$.

In compression test $\left(\sigma_3 = 0,\ \tau_n = \sigma_1\sin\alpha\cos\alpha;\ \sigma_n = \sigma_1\cos^2\alpha\right)$ we obtain from eq.12

$$dA_p = P\delta l_p = \sigma_1\delta\varepsilon_1^p V_0 = 2a\sigma_1\cos\alpha\left(\sin\alpha + \frac{\sqrt{2}}{\pi}\cos^2\alpha\left(\sin\alpha - \mu\cos\alpha\right)\right)db \qquad (13)$$

where $V_0 = HB$ is a representative volume. Taking into account

$$d\hat{\gamma}^p = \frac{1}{V_0}\int d\gamma^p dV = \frac{2a\delta b}{V_0}; \qquad d\hat{\theta}^p = (1-2\nu)\delta\varepsilon_1^p \tag{14}$$

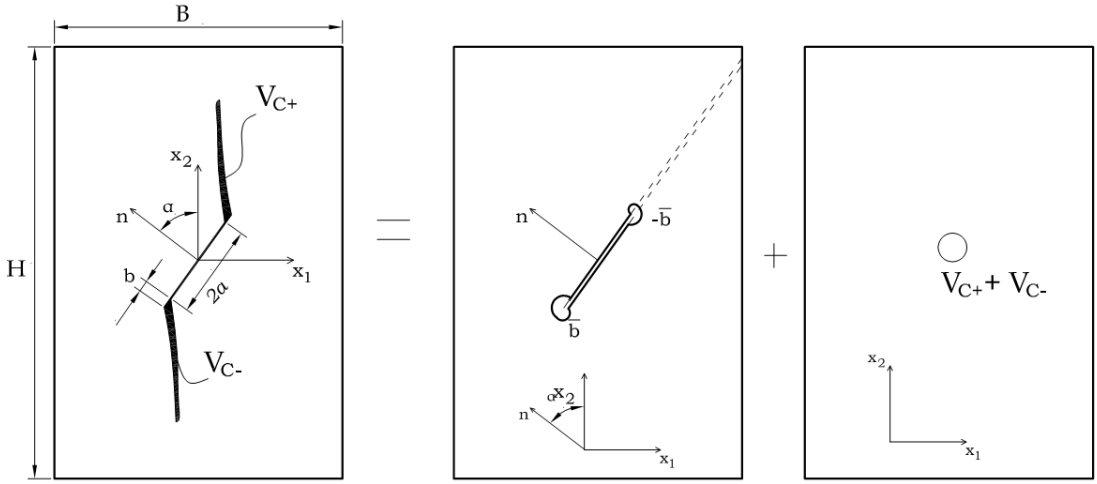

Fig.10. The stress states superposition.

we obtain the dilatancy coefficient in the range *(0,4…..1)*

$$\beta = d\hat{\theta}^p / d\hat{\gamma}^p = \frac{1-2\nu}{f(\mu)}, \tag{15}$$

where $f(\mu)$ is a function which takes into account all active wing cracks $(d\tau_{eff} = d\tau_n - \mu\, d\sigma_n > 0)$ *or* $\psi < \alpha < \pi/2$.

SHEAR TEST RESULTS

The shear tests were conducted in-situ (Svalbard, 2014-2018). The samples with two necks (photo 2) were cut from the floating sea ice sheet and loaded by hydraulic jacks through the steel slab or semicylinder. The shear fault was the predominant failure type for ice in the shear, as it was observed during field research, but sometimes the shear faulting on the neck couldn't occur, the sample failed by crushing or punching mode (Photo 3, 4). This phenomena was named shear collapse. Shear faulting in the ice is usually observed under uniaxial loading, the fracture surfaces are inclined 30^0 or over to the loading direction and owing to the sliding one piece of ice over the other (Schulson, 1991).

Table 2. Shear test result (in-sity Svea buhta, Barents Sea)

Date	# test	Length l [cm]	Thickness h [cm]	Temperature, ^{0}C	Salinity, ppt	Ultimate force, kN	Shear strength, kPA	Tensile strength*, kPa
29.03.2014	#1	25	43	-5.0	6.0	85	395**	98
14.03.2015	#2	22	71	-2.2	4.7	54***	172	81
03.03.2016	#3	25	58	-2.6	4.0	213	734	150
08.03.2016	#4	25	58	-2.4	4.4	218	751	144
24.03.2017	#5	20	57	-5.0	6.0	214	940	102..128

* Tensile strength was determined on the same ice floe and in the same conditions (salinity, profile of ice temperature and strain rate $\approx 10^{-3}\, s^{-1}$) in full-scale tests;

**Failure mode #1test is punching;

*** Necks failure occurred not simultaneously.

Comparing Table 2 with the results of Saeki tests (table 1) it's seen, that shear strength in our full-scale tests is significantly higher (#3,#4 - two times and #5 more than 1.5). Our proposal is that self-confinement effect takes place in these shear tests and the loading trajectory follows the trace OAB on fig.7.

Photo 2

Photo 3

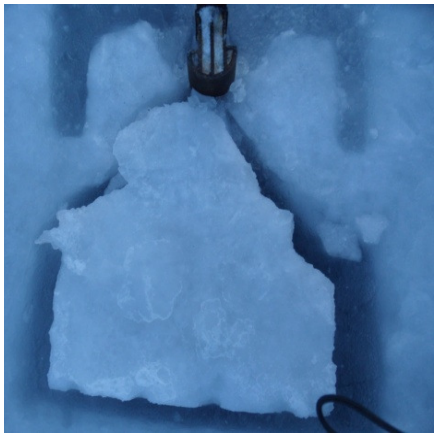

Photo 4

Photo2. Shear fault in the necks (Test #3 Table 2)

Photo3. (Test #1 Table 2

Photo 4. The sea ice sample in test #1 was punching.

Stress distribution from the FEM simulation typical test #3, #4 is representing on fig.11b, 11c. Shear fault line in both tests inclines to axe of neck with angle ≈23^0 (fig. 11a). It means that coefficient of dilatancy is more than $\beta > ctg67^0 = 0{,}42$.

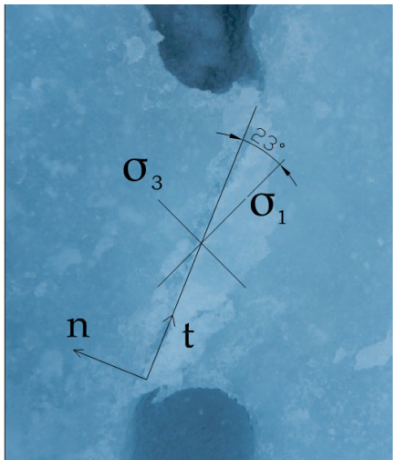

(a)

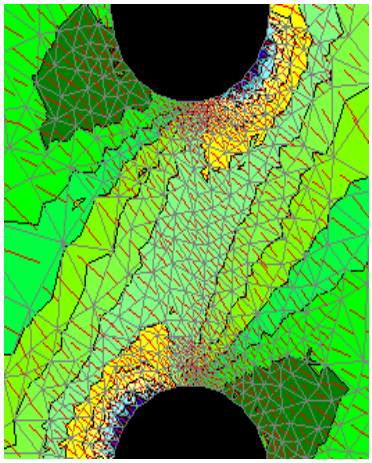

(b)

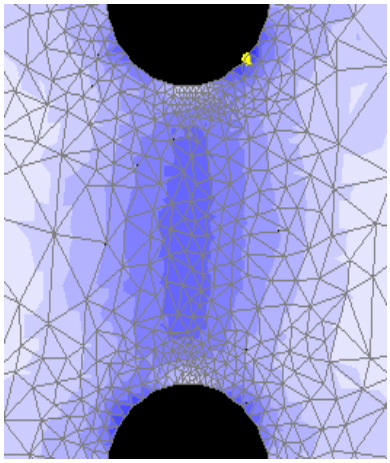

(c)

Fig.11 (a)- schema test#1 with shear fault (photo2), (b) trajectory of the principal stress σ_3 on the neck area, (c) central area of uniform shear.

The wing crack mechanism takes place in the central area of uniform shear $\sigma_1 = -\sigma_3 = \tau$ (fig.11c). Spalling events are observed in the compression area near free surface of the hollow chamfer. During simulation the dilatancy was modeled "step by step" as a thermal dilation in those elements, where the condition of active process (6) took place.

If we return to the test #1 result (photo 3) we mention that the punching force is in accordance with the tensile strength $F_{punch} = \frac{\sigma_t}{\cos^2 \alpha} A = 98kN$ and is in a good agreement with the ultimate force 85kN in test. According (9) the dilatancy coefficient from our tests could be estimated by inequality $0.42 < \beta < 1$.

SUMMARY AND CONCLUSIONS

Full-scale tests examination of the sea ice shear fracture at strain rate $\approx 10^{-3}$ s^{-1} and lower has led to the following conclusions:

- The shear strength shows the significant dependence on the self-confinement effect. Shear strength values are significantly higher than shear strength obtained in direct shear tests (Saeki, et al. 1985);
- Shear fault and punching failure are the common sequences in collisions of the sea ice failure under shear;
- Shear tests give the possibility to estimate the dilatancy coefficient in a range $0.42 < \beta < 1$.

The theoretical observation displays the productivity of both macro- and microstructure concepts. In the frame of macroscopic incremental theory of dilatant hardening material it is shown that:

- The self-confinement effect increases the ultimate strength due to appearance lateral compression stress;
- Shear fault and punching are the two types of the failure mode in shear tests under confinement. The dilatancy process dictates and determines the strength. If a sample geometry satisfies $ctg\alpha < \beta$ than lateral compression strength occurs and ultimate load increases significantly in comparison with the pure shear strength. If $ctg\alpha > \beta$ than it will be punching process and tensile strength will dictate the ultimate load.

In the frame of microscopic concept, based on "wing-crack" mechanism, the dilatancy coefficient is estimated as a function of Poisson ratio and coefficient of internal friction only.

ACKNOWLEDGEMENTS

The authors wish to acknowledge the support of the Research Council of Norway through the Centre for Sustainable Arctic Marine and Coastal Technology (SAMCoT) and AOCEC project of IntPart program.

REFERENCES

Ashby, M.F. and S. D. Hallam, 1986. The failure of brittle solids containing small cracks under compressive stress states. Acta Metallurgica et Materialia, 34, 497–510.

Barenblatt, G.I. and Cherepanov, G.P., 1960. On the wedging of brittle bodies. Journal of Mechanics and Applied Mathematics, 23,993–1014.

Butkovich T.C. 1956. Strength of ice, SIPRE, Research report RR-20. Willmate, Illinois, 15p.

Frederking, R.M.W., Timco, G.W. 1984. Measurement of shear strength of granular /discontinous-columnar sea ice. Cold Regions Science and Technology. Vol. 9, No. 9, pp. 215–220.

Frederking, R.M.W., Timco, G.W. 1986. Field measurements of the shear strength of columnar-grained sea ice. Proceedings 8th IAHR Symposium on Ice, vol. I, pp. 279–292. Iowa City, U.S.A.

Frederking, R.M.W., Svec, O., Timco, G.W., 1988. The shear strength of ice. Proceedings 9th IAHR Symposium on Ice, vol. 3, pp. 76–88, Sapporo, Japan.

Golding, N., S.A. Snyder, E.M. Schulson and C.E.Renshaw. Plastic faulting in saltwater ice. Journal of Glaciology, 60(221), doi:10.3189/2014/JoG13J178.

Laurence D. Wesley. Fundamentals of Soil Mechanics for Sedimentary and Residual Soils, John Wiley & Sons, 2009, 464 p.

Lehner F., M.Kachanov. (1996). On modeling of "winged" cracks forming under compression. International Journal of Fracture, 77: 65–75.

Marchenko, A., Karulin, E., Chistyakov, P., Sodhi, D., et al. 2014. Three dimensional fracture effects in tests in cantilever and fixed ends beams, 22nd IAHR International Symposium on Ice, Singapore, 7 pp.

Rice, J. (1975). On the stability of dilatant hardening for saturated rock masses. Journal of Geophysical Research, 80(11), 1531-1536.

Rist, M.A., S.J. Jones and T.D.Slade, 1994. Microcracking and shear fracture in ice. Annals of Glaciology, ., 19, 131-137.

Rudnicki J. W. and J. R. Rice. 1975. Conditions for the localization of deformation in pressure-sensitive dilatant materials. Journal of the Mechanics and Physics of Solids, 23, 371–394.

Saeki, H., Ono, T., En, N., and Naok, N. (1985). Experimental study on direct shear strength of sea ice. Ann. Glaciol., 6(1), 218–221

Schulson, E.M. 2001. Brittle failure of ice. IUTAM Engineering Fracture Mechanics, 68, 1839-1887

Schulson, E. M. 2002. Compressive shear faulting in ice: Plastic versus Coulombic faults. Acta Materialia, 50:3415–3424.

Schulson, E. M. 2004. Compressive shear faults within Arctic sea ice: Fracture on scales large and small. Journal of Geophysical Research, 109, doi:10.1029/2003J002108.

Schulson, E.M., A.L.Fortt, D.Iliescu, and C.E.Renshaw. 2006, Failure envelope of first-year Arctic sea ice: The role of friction in compressive fracture, Journal of Geophysical Research, II, C11S25, doi:10.1029/2005JC003235

Schulson, E.M., A.L.Fortt, 2012, Friction of ice on ice. Journal of Geophysical Research, v.117, Issue B12, doi: 10.1029/2012JB009219

Tada, H., P. C. Paris and G. R. Irwin, 2000. The Stress Analysis of Cracks Handbook, 3-d Edition, ASME, 696p.

Timco, G. W., and W. F.Weeks, (2010). A review of the engineering properties of sea ice. Cold Regions Science and Technology, 60(2), 107–129

Tremblay, L.M., L.A.Mysak (1997). Modelling sea ice as a granular material, including the dilatancy effect, Journal of Geophysical Research, 27, 2342-2360.

Wilchinsky, A.V. and D.Feltham, (2011) Modeling Coulombic failure of sea ice with leads. Journal of Geophysical Research, 116 (C8). C08040. Doi:10.1029/2011JC007071.